

DOI: 10.1070/QEL16155

Study of the formation of a microrelief on ZnSe- and CdSe-crystal surfaces ablated by excimer KrF-laser radiaton

S.K. Vartapetov, A.V. Zakhryapa, V.I. Kozlovsky, Yu.V. Korostelin, V.A. Mikhailov, Yu.P. Podmar'kov, I.Yu. Porofeev, D.E. Sviridov, Ya.K. Skasyrsky, M.P. Frolov, I.M. Yutkin

Abstract. **One-dimensional gratings with a period of 0.5–2.3 μm are formed on the surfaces of CdSe and ZnSe crystals ablated by two interfering radiation beams of a nanosecond excimer KrF laser. Investigated are the dependences of the shape and depth of gratings on the energy density under irradiation by a single pulse, and on the number of pulses at a given energy density. The maximum grating depth is estimated as ~0.57 of the period. By forming a one-dimensional grating with a period of 1.5 μm and a depth of 0.53 μm on the CdSe-crystal surface, this surface becomes antireflective at a wavelength of 4 μm. The surface reflectivity is reduced by 88%. A possibility of forming two-dimensional gratings having periods of 1 and 1.5 μm is demonstrated.**

Keywords: *antireflection surface micro-relief, mid-IR range, II–VI crystals, laser ablation, excimer KrF laser.*

1. Introduction

Formation of an antireflection (AR) microrelief on the surface of optical elements is of considerable interest for a number of applications, particularly in high-power mid-IR lasers. If we compare this method with conventional deposition of thin-film AR coatings on the surfaces of optical elements, the surface relief AR microstructures can significantly increase the radiation strength of the AR surface and its resistance to external operating conditions, and also increase the angular and spectral width of the AR curve [1–3]. AR microstructures are commonly formed by using a multistage expensive technology, which involves photolithography and dry etching in plasma. Another method for producing a microrelief on the optical element surface is laser ablation. This method is well studied and tested on a number of materials, including metals, alloys, glasses and some semiconductors [4–12]. To a lesser extent, laser ablation has been investigated for ZnSe crystals and other II–VI compounds [13, 14]. Recently, using a variety of compounds of this type, doped by the divalent ions of transition metals (ZnSe:Cr, ZnSe:Fe, CdSe:Cr, etc.), efficient optically pumped mid-IR lasers have been developed, operating both in the pulsed and cw regimes [15–19] and possessing a significant potential for practical applications [20, 21]. In this regard, of undoubted interest is the development of the methods of deposition of broadband AR coatings on the surfaces of laser elements on the basis of II–VI crystals, which allow the losses to be minimised both at the pump wavelength and in a broad (~1 μm) spectral range of lasing, while maintaining the radiation resistance of the material.

The aim of this work is to study the shape and depth of one-dimensional gratings formed in the ablation of the material under the action of two interfering beams of an excimer KrF laser.

2. Experiment

One-dimensional spatially periodic structures with an arbitrary period are formed on the sample according to the scheme shown in Fig. 1.

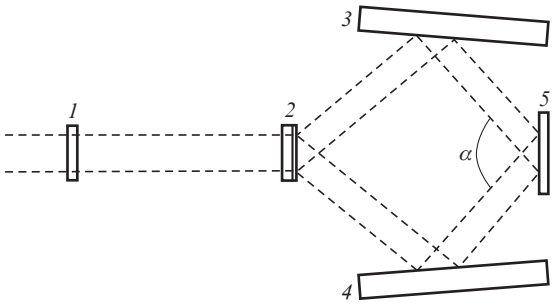

Figure 1. Schematic of the interferometer: (*1*) cylindrical lens; (*2*) phase mask; (*3*) and (4) reflecting mirrors; (*5*) sample.

The laser beam passes through cylindrical lens (*1*) and splits into two beams by phase grating (*2*). Then, using reflecting mirrors (*3*) and (*4*), the beams are converged in the plane of sample (*5*) at an angle α. The laser energy density at the sample is varied by moving the cylindrical lens along the optical axis. The interference pattern period p in the sample plane is varied by selecting the angle α in accordance with the formula

S.K. Vartapetov, V.A. Mikhailov, I.Yu. Porofeev Physics Instrumentation Centre, A.M. Prokhorov General Physics Institute, Russian Academy of Sciences, 142190 Moscow, Troitsk, Russia;
A.V. Zakhryapa, I.M. Yutkin Russian Federal Nuclear Center 'All-Russian Research Institute of Experimental Physics', prosp. Mira 37, 607188 Sarov, Nizhnii Novgorod region, Russia;
V.I. Kozlovsky P.N. Lebedev Physics Institute, Russian Academy of Sciences, Leninsky prosp. 53, 119991 Moscow, Russia; National Research Nuclear University 'MEPhI', Kashirskoe sh. 31, 115409 Moscow, Russia; e-mail: vikoz@sci.lebedev.ru;
Yu.V. Korostelin, Yu.P. Podmar'kov, D.E. Sviridov, Ya.K. Skasyrsky, M.P. Frolov P.N. Lebedev Physics Institute, Russian Academy of Sciences, Leninsky prosp. 53, 119991 Moscow, Russia

Received 9 June 2016
Kvantovaya Elektronika **46** (10) 903–910 (2016)
Translated by M.A. Monastyrskiy

$$p = \frac{\lambda}{2\sin(\alpha/2)}. \quad (1)$$

As a radiation source, we have used a CL7500 excimer laser system (Optosystems Ltd.), whose optical scheme is shown in Fig. 2. It consists of two identical gas-discharge modules (*1*) and (*2*) (KrF lasers of CL7000 series) and optical blocks (*3*) and (*4*) placed on a common optical table, as well as of control and synchronisation systems. Module (*1*) operates as a master oscillator (MO), and module (*2*) – as a power amplifier (PA). As discharge chamber windows of the laser modules, use is made of a monocrystalline MgF_2, which is placed at the Brewster angle to the optical axis of the laser module to minimise the intracavity losses. The active medium length of a single module is 600 mm, and the height is 22 mm.

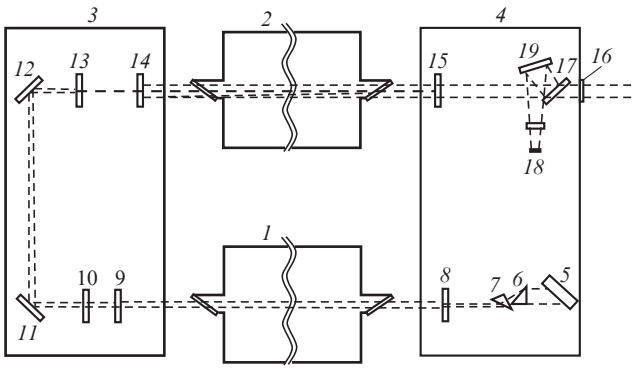

Figure 2. Optical scheme of a SL7500 excimer laser system: (*1*) MO; (*2*) PA; (*3*, *4*) optical blocks; (*5*) grating; (*6*, *7*) prism telescope; (*8*, *9*, *13*) apertures; (*10*) output mirror; (*11*, *12*, *19*) deflecting mirrors; (*14*) concave spherical mirror; (*15*) convex spherical mirror; (*16*) exit window; (*17*) beam splitter; (*18*) energy meter.

The MO resonator consists of two-prism telescope (*6*, *7*) with a magnification factor of 14, Echelle diffraction grating (*5*) (600 lines mm^{-1}, blazing angle of 54.09°) and output mirror (*10*) with a reflection coefficient of 20%. For better spatial selection of radiation, diaphragms (*8*, *9*, *13*) have been installed. The use of a diffraction grating as a one of the mirrors allows the width of the generation line to be reduced down to 0.0015 nm (increasing the coherence length up to 15 mm).

The unstable PA resonator consists of concave spherical mirror (*14*) with a radius $R = 3.532$ m and output convex spherical mirror (*15*) with a radius $r = 0.3$ m. A through hole with a diameter of 1.5 mm is made in the concave mirror to introduce the MO radiation into the PA active medium. A beam with a diameter of 1.5 mm, when passing through the interelectrode gap, is incident on the convex spherical mirror of the cavity and, having reflected from it, passes again through the PA active medium. The beam is already divergent at this stage, so that it completely overlaps the cross section of the active medium on the concave mirror of the cavity. Then, the beam is reflected from the concave mirror, and then, after the last amplification within the active gaseous medium, comes out of the laser system through aperture (*16*). An insignificant fraction of the laser beam, after reflection from beam splitter (*17*), falls on energy meter (*18*).

The distance b between the PA resonator mirrors is calculated by the formula

$$b = \frac{R - r}{2}, \quad (2)$$

which ensures the planarity of the output beam front. In our case, $b = 1616$ mm. The radii of the mirrors are chosen to optimally fill the laser's active volume by radiation. The important resonator characteristic is also the telescoping ratio M defined as

$$M = \frac{R}{r}. \quad (3)$$

The greater the M, the smaller the divergence and the greater the length of spatial coherence of the laser beam, but, at the same time, the lower the output energy of the amplified pulse. In our case, $M \approx 12$. The use of a telescopic cavity allowed reducing the radiation divergence down to 0.2 mrad [22]. The total pulse energy constituted 250 mJ, the duration was 20 ns, the pulse repetition rate reached 100 Hz and the laser generation wavelength was equal to 248 nm. The maximum size of the irradiated area on the sample surface was 6×20 mm. To decrease the area size, the beam was diaphragmed.

We have used undoped ZnSe single-crystal plates of different crystallographic orientation, and also ZnSe : Fe and CdSe : Cr plates with the dopant concentration of $\sim 10^{18}$ cm^{-3}. The plate thickness was 1.5 mm. The plate surfaces were mechanically polished. In some of the plates, the damaged layer, after mechanical polishing, was removed using a polishing etchant on the basis of CrO_3 solution in HCl. The surfaces of the plates with a microrelief were studied by means of a Solver P-47 Pro (NTMDT) scanning probe microscope. We have also used HA-NC (NTMDT) probes having a cone-tapered tip with a length of 1.5 μm and an apex angle of 30°. Figure 3 shows a scan of the TGZ3 reference grating with vertical walls. It is seen that the probe width is less than 500 nm at a height of 540 nm from the tip. The ratio of the probe height to its width exceeds the corresponding ratio for the grooves in the microstructures obtained. This indicates that the probe shape does not affect the resulting images. All measurements were performed in the contact scanning mode.

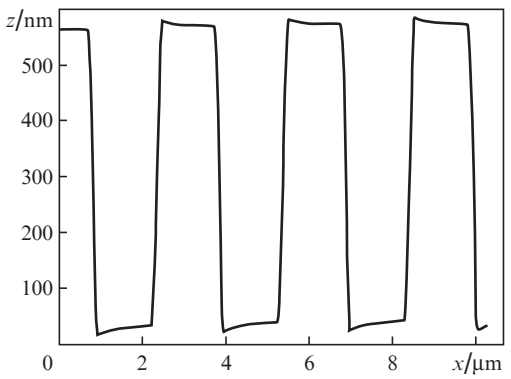

Figure 3. Scanned image of a reference grating with a period of 3 μm and a depth of 540 nm.

The transmission spectra of the samples were measured using an FSM 2201 IR Fourier spectrometer (Infraspek Ltd.).

3. Results of the experiment

Figure 4 shows the shapes of a grating formed on the surface of a CdSe : Cr crystal under single-pulse irradiation at different energy densities of laser radiation. The interference irradiation zone was 8 mm in length and 1.5 mm in width. The energy density distribution within the irradiation zone was nonuniform. In particular, a modulation arising from diffraction on the aperture edge was observed at the zone edges. In addition, the grating contrast (a ratio of the depth of dips to the grating period) was varied irregularly over the surface of the irradiation zone (approximately by 1.5 times). A possible reason for such a nonuniformity is a macro-nonuniform intensity distribution within the laser beam. However, by selecting each time the image areas with a maximum contrast, it is possible to reveal a certain regularity in the varying grating shape and contrast depending on the irradiation energy density.

The image of the original surface (Fig. 4a) contains the traces of mechanical polishing. These traces disappear after chemical polishing. At a small excess of the ablation threshold, the grating has fairly narrow grooves (of width 0.6 μm in Fig. 4b) with the side ribs protruding above the original surface. The appearance of ribs is associated with extrusion of the near-surface molten crystal layer from the zone with a high density of absorbed energy into the zone with a lower energy density by the pressure of the near-surface plasma formed in the process of crystal ablation [11]. With a further increase in laser energy density, the width of the grooves increases, and the height of ribs grows (Fig. 4c) until they merge to form grating vertices (Fig. 4d).

One can see from Fig. 4 that the volume of ribs is substantially less than that of grooves. Given the vertical location of the sample, the remaining ablation products are mostly dissolved in surrounding air and only partially deposited on the grating surface. The maximum grating depth is achieved at the radiation energy density of $F \approx 140$ mJ cm^{-2} and constitutes ~220 nm. A further increase in energy density reduces the grating depth and contrast; therefore, the grating profile remains close to sinusoidal. At $F = 500$ mJ cm^{-2}, the grating depth is only a few tens of nanometers (35 nm in Fig. 4e). The contrast decrease is probably explained by the fact that, due to insufficiently high contrast of the interference pattern of two laser beams, the ablation threshold is also achieved at the minima of the interference pattern. On the other hand, the plasma formed at the maxima of the interference pattern starts to shield the crystal surface from incident radiation, thereby reducing the ablation rate.

In the case of a small depth of the grating formed at a large F, the nanoscale hillocks emerging on the laser-treated surface become visible. This is particularly well seen in the image presented in Fig. 5 obtained in the regime of lateral force microscopy (friction forces), when, along with the surface topography (Fig. 5b), torsional bending of the cantilever is recorded. The characteristic transverse size of hillocks is 50 nm, and their height amounts to 40 nm. The surface density of hillocks is estimated as 5×10^8 cm^{-2}. The origin of these hillocks is not yet clear. It is possible that the deposition of ablation products results in the formation of nano-objects of type of quantum dots [7].

Because the grating groove depth obtained in a single pulse is limited to ~220 nm at a period of 2.3 μm, we have tried to increase that depth by using multiple pulses. Figure 6 presents the shapes of gratings at different numbers of pulses for the irradiation energy density of 100 mJ cm^{-2}. The pulses followed with a repetition rate of 10 Hz.

The maximum grating depth was obtained under irradiation by five pulses and amounted to 835 nm, which exceeds one-third of the grating period. We should also note that this depth is nearly five times greater than the grating depth resulting from single-pulse irradiation. However, the depth starts to decrease when the number of pulses increases. The main reason for that is apparently a temporal drift of the sample position relative to the interference pattern. In addition, the shape of the groove bottom is rather complicated and varies along the grating grooves (see the image in Fig. 6c). It is likely that certain problems with ejection of ablation products from the grooves arise in the case of a sufficiently large depth [9].

Similar results were obtained in the formation of gratings on the ZnSe : Fe and ZnSe surfaces. Figure 7 shows the dependence of the depth of a grating with a period of 1.5 μm on the number of pulses irradiating the ZnSe surface and following with a repetition rate of 100 Hz. As in the case of CdSe : Cr, a rapid saturation of this dependence is observed, although we have not revealed any noticeable decline in it when the number of pulses amounts to 10–100. It is possible that the drift of the interference pattern along the sample surface irradiated by a large number of pulses at a pulse repetition rate of 100 Hz has lesser influence on the grating contrast than at a pulse repetition rate of 10 Hz (Fig. 6). The maximum grating depth was achieved under irradiation employing 100 pulses with $F =$ 100 mJ cm^{-2} and constituted 850 nm. Note that we have not found any significant differences in the microrelief of the gratings formed on the surface of (001) and (111) crystals.

An example of a grating with a smaller (1.5 μm) period, formed on the CdSe : Cr surface using five pulses at $F =$ 140 mJ cm^{-2}, is presented in Fig. 8. Here, the groove depth was ~540 nm. The gratings with a period of 0.5 μm were also formed. In the case of single-pulse irradiation with $F =$ 100 mJ cm^{-2}, the groove depth on the ZnSe surface was 60 nm.

Figure 9a shows a three-dimensional image of a two-dimensional grating on the ZnSe surface. Initially, a one-dimensional grating with a period of 1.5 μm was formed under single-pulse irradiation with $F = 140$ mJ cm^{-2}; then, the sample was rotated by 90° and a second one-dimensional grating was formed. The height difference in the thus formed microrelief was ~300 nm. To increase this difference, it is necessary to increase the number of pulses which are used in the formation of a one-dimensional grating. For example, Fig. 9b shows a similar grating formed by two crossed gratings with a period of 1 μm each, which were formed by ten pulses at $F =$ 125 J cm^{-2}. The height difference in this two-dimensional grating exceeds 500 nm.

4. Discussion of the results

An AR microrelief can be formed in two ways. The first way is based on the working mechanism of single-layer AR coatings with a refractive index $n_{ar} = \sqrt{n_{cr}}$ and a thickness $\lambda/(4n_{ar})$, where n_{ar} and n_{cr} are the refractive indices of the AR coating and crystal, respectively [1]. In this case, a layer with an approximately constant thickness and a refractive index n_{ar} averaged along the layer is formed on the crystal surface. In

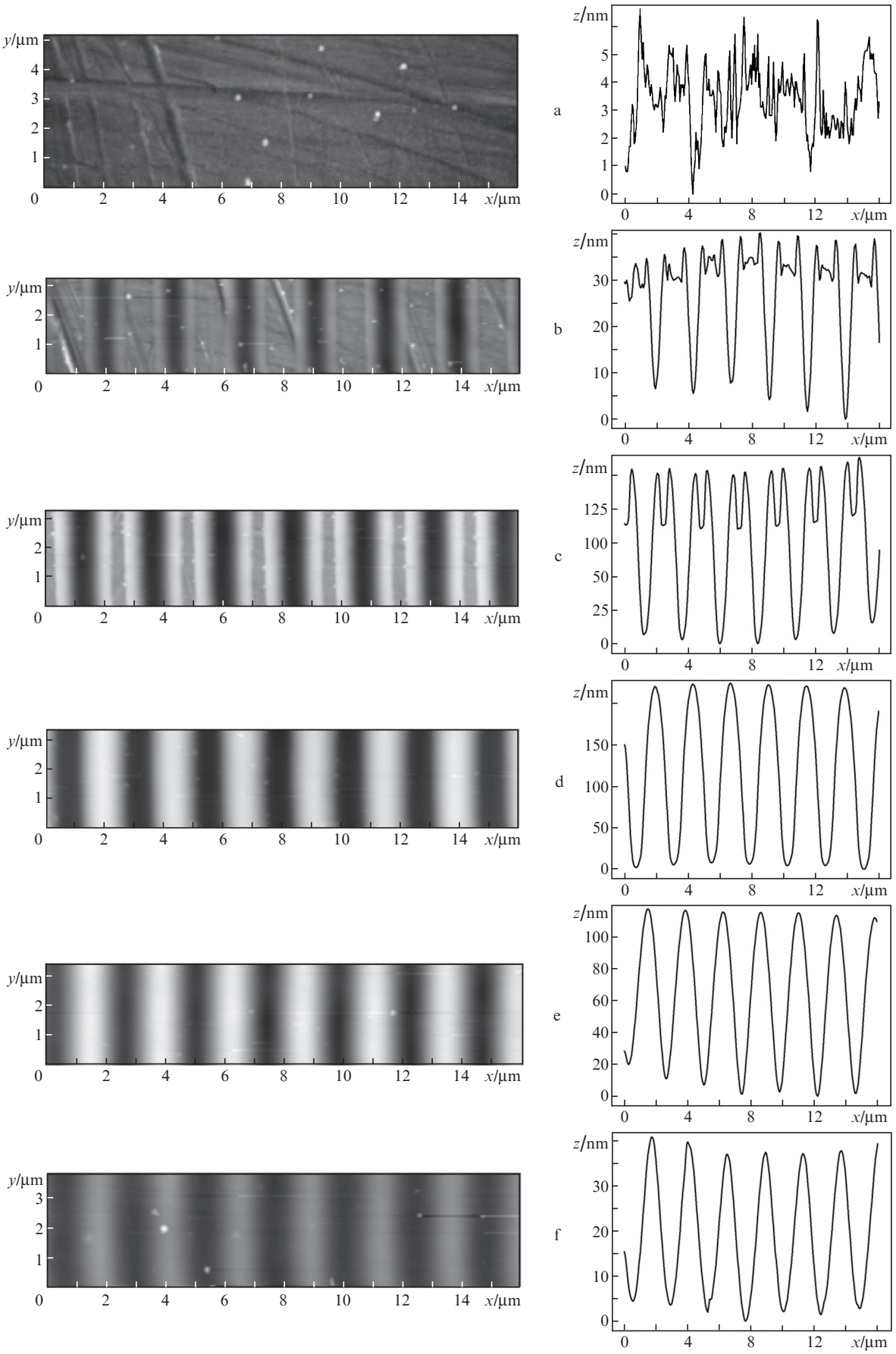

Figure 4. Image fragments of a grating on the CdSe : Cr surface, formed under irradiation by a single pulse with an energy density F = (a) 0, (b) 80, (c) 100, (d) 140, (e) 200 and (f) 500 mJ cm^{-2}. To the right of images, the corresponding, vertically-averaged, grating profiles are presented.

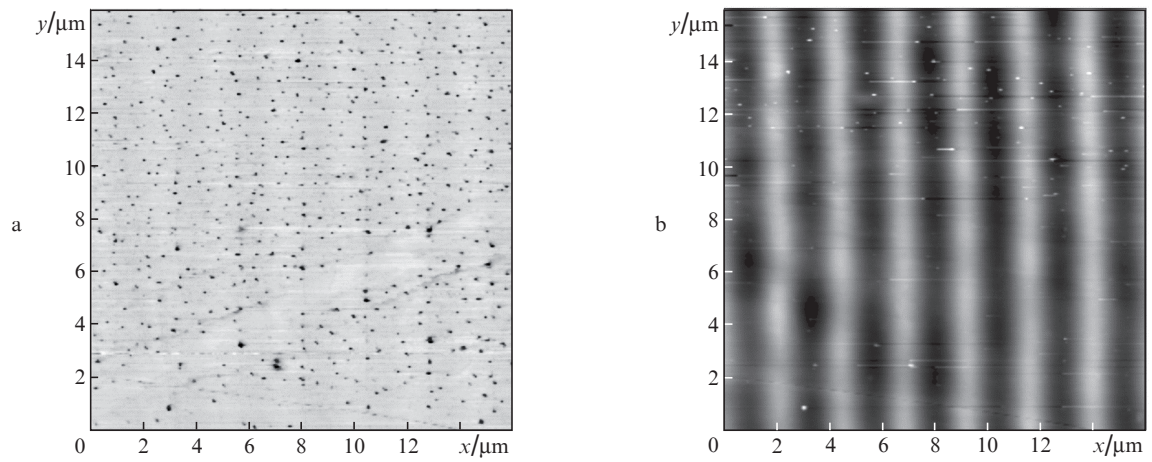

Figure 5. (a) Image of the CdSe : Cr crystal surface, obtained in the regime of lateral force microscopy and (b) the corresponding topographic image after irradiation by a pulse with $F = 500$ mJ cm^{-2}. Dark peaks are revealed against the background of the low-contrast grating with a period of 2.3 μm.

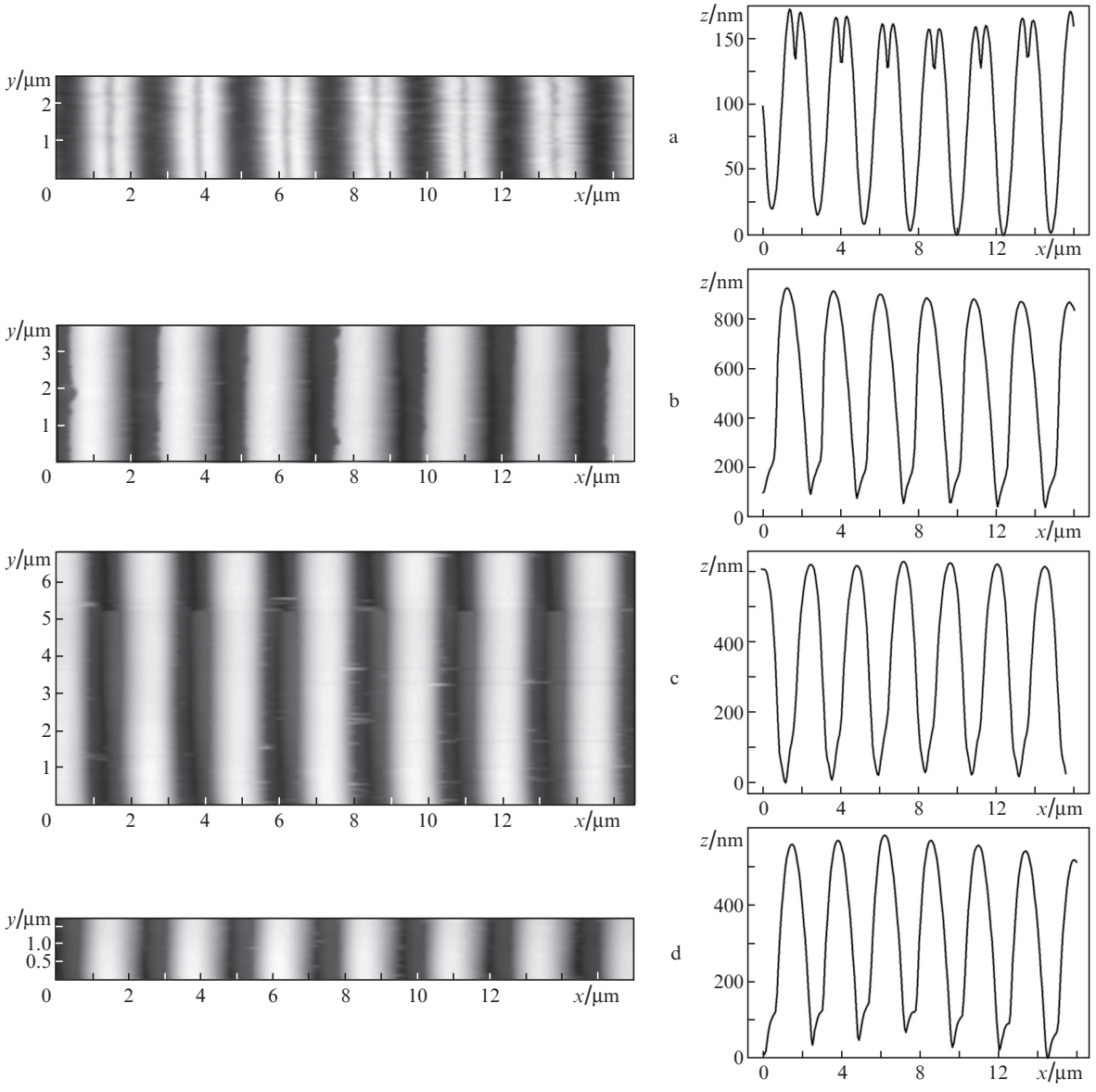

Figure 6. Image fragments of the gratings formed on the CdSe : Cr surface irradiated by (a) 1, (b) 5, (c) 20 and (d) 100 pulses with $F = 100$ mJ cm^{-2}, which follow with a repetition rate of 10 Hz. To the right of the images, the corresponding, vertically-averaged, grating profiles are presented.

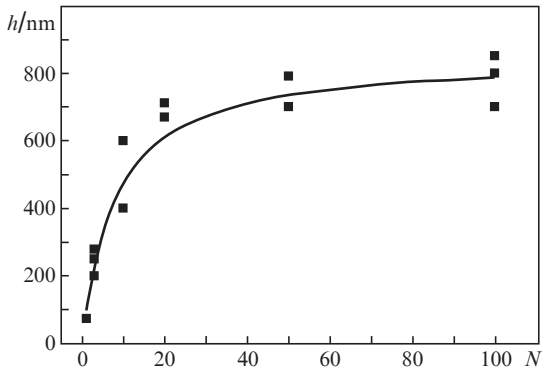

Figure 7. Grating depth h with a period of 1.5 μm on the ZnSe crystal surface as a function of the number of pulses N at $F = 100$ mJ cm^{-2} and a repetition rate of 100 Hz.

particular, this layer may contain holes of various shapes or grooves with vertical walls, the characteristic sizes of which are smaller than the AR microrelief wavelength. In this case, the proportion γ of the crystal surface occupied by these holes or grooves must satisfy the condition

$$\sqrt{n_{cr}} = n_{cr}(1-\gamma) + n_a\gamma \qquad (4)$$

and for $n_{cr} = 2.4$ (ZnSe), $n_a = 1$ (air) is equal to 0.61. Besides, to avoid the diffraction and scattering losses (including those inside the crystal), the holes or grooves must be arranged regularly on the surface, with a period less than λ/n_{cr}. In this case, we will have a one-dimensional or two-dimensional grating in which the depth h of grooves and holes may only constitute $n_{cr}/(4n_{ar}) = 0.39$ of the period p. However, the formation of holes and grooves with vertical walls and a strictly defined depth (with a flat bottom) is a challenging technological task. A substantial deviation from these requirements increases the radiation scattering loss. However, one may count on a significant, though not perfect, antireflection. In particular, the grating shown in Fig. 6b (period is $p = 2.3$ μm, depth is $h = 0.835$ μm, $h/p = 0.36$) and Fig. 8 ($p = 1.5$ μm, $h = 0.535$ μm, $h/p = 0.36$) may exhibit the AR effect. The maximum grating

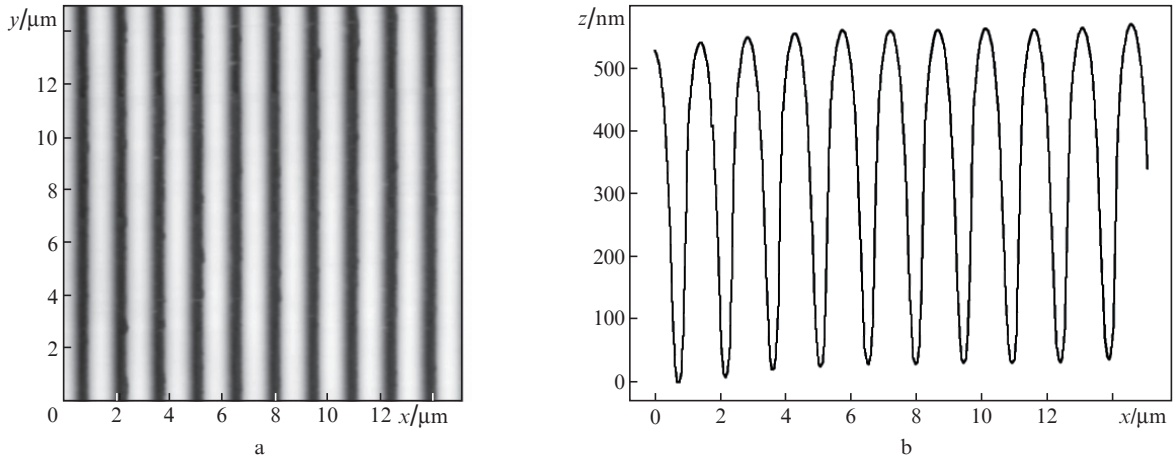

Figure 8. (a) Image of the grating with a period of 1.5 μm on the CdSe:Cr surface, formed by five pulses at $F = 140$ mJ cm^{-2}, and (b) vertically-averaged grating profile.

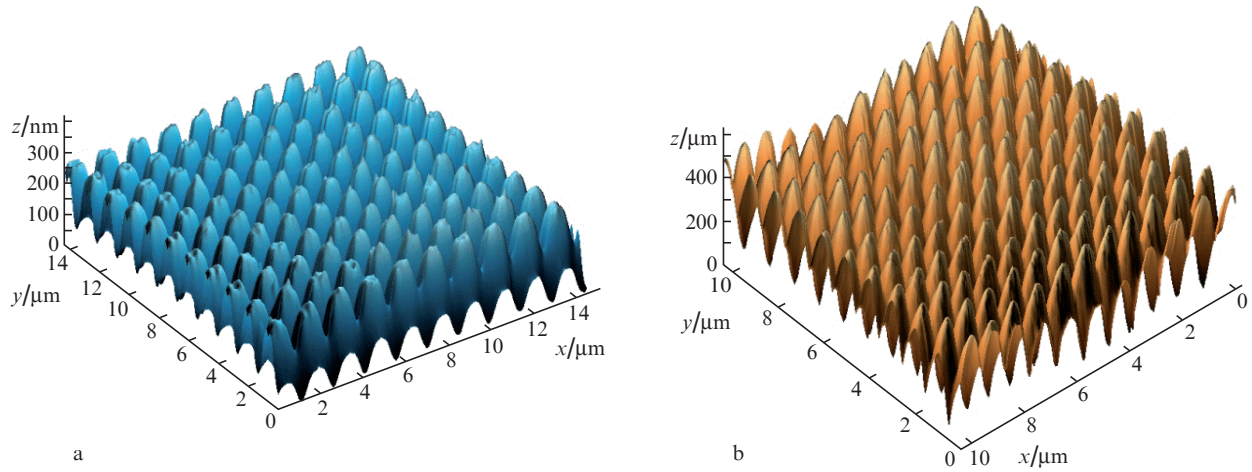

Figure 9. Images of a two-dimensional grating on the ZnSe surface, resulting from a superposition of (a) two one-dimensional gratings with a period of 1.5 μm, formed by a single pulse at $F = 140$ mJ cm^{-2}, and (b) gratings with a period of 1 μm, formed by ten pulses with $F = 125$ mJ cm^{-2}.

contrast $h/p = 0.57$ was achieved on the ZnSe surface (see Fig. 7).

Figure 10 shows the IR transmission spectra of the original CdSe:Cr crystal and the crystal with a grating (p = 1.5 μm) on one of its surfaces (see Fig. 8). One can see a significant difference between these spectra, which is associated with a partially antireflective crystal surface with a grating at a wavelengths near 4 μm. In the long-wavelength region the spectra virtually coincide, since the microrelief corresponding to the long-wavelength radiation is not deep enough. In the short-wavelength region, at $\lambda < 3.6$ μm, the losses are increased due to diffraction of incident radiation on the grating. In the case of an ideal AR microstructure, the transmittance in the area of 4–5 μm should increase by 12.3% (see the inset in Fig. 10). For a crystal with a grating under consideration, we observe an increase of 10.9% in transmittance, which means that the crystal has a fairly strong, though not ideal, AR microrelief.

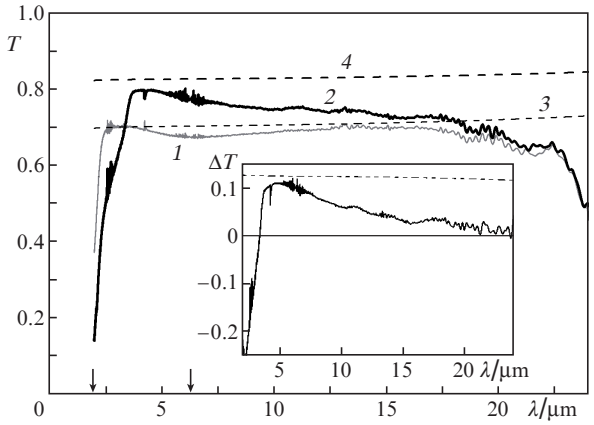

Figure 10. Transmittance spectra T of (*1*) the original CdSe:Cr crystal and (*2*) the crystal with a grating on one of its surfaces, and also the calculated transmittance spectra for (*3*) a pure CdSe crystal with Fresnel reflection from both surfaces and (*4*) a crystal with an ideal AR coating from one of its sides with allowance for refractive index dispersion. The arrows indicate the position of Cr absorption lines. The inset shows the corresponding difference ΔT in the transmission spectra of CdS:Cr crystals with a grating and without it.

We should note that the microrelief described allows increasing the radiation strength of an active laser crystal, but, as in the case of conventional single-layer AR coatings, the corresponding spectral and angular widths are rather small.

The second way is based on the formation of a two-dimensional array of pyramids (Motheye microstructure) [1–3]. The shape of the pyramids is also important, although the most important factor is the large depth of the relief (up to the doubled period of the structure). As has been shown by experiments, an increase in the grating depth by more than 1/10 of the grating period cannot be attained by increasing the irradiation energy density in a single pulse. More promising is to increase the number of pulses at a small excess of the ablation threshold in each pulse. Preliminary experiments have demonstrated that the relief contrast $h/p = 0.57$ is reachable within the framework of this method. A further increase in contrast is probably associated with the problem of removal of ablation products from deep grooves.

5. Conclusions

Using the laser ablation method, we have formed periodic one-dimensional gratings with a period of 0.5–2.3 μm on the surfaces of CdSe:Cr, ZnSe:Fe and ZnSe crystals. We have used the interference of two laser beams from a nanosecond excimer KrF laser, providing a radiation energy density of 500 mJ cm^{-2} per pulse. The ablation threshold was slightly less than 80 mJ cm^{-2}. The maximum grating depth reachable in a single pulse amounted approximately to 1/10 of the grating period at a moderate energy density $F \approx 140$ mJ cm^{-2}. The relief contrast decreases with increasing F. At F = 500 mJ cm^{-2}, nanoscale formations, i.e. quantum dots with a typical size of a few tens of nanometers and a density of 5×10^8 cm^{-2}, are observed on the crystal surface. The maximum grating depth was achieved under irradiation using a series of pulses with an energy density $F \approx 100$ mJ cm^{-2}, which corresponds to a slight excess of the ablation threshold and amounted to 0.57 of the grating period. A further increase in the grating depth is probably associated with the problem of removal of ablation products from deep grooves. A possibility of formation of two-dimensional gratings with periods of 1 and 1.5 μm is demonstrated. The proposed method can be employed in the case of mid-IR lasers to form a partially antireflection microrelief on the active elements of CdSe and ZnSe doped by the transition metals of Cr and Fe. More research is needed to ensure an increase of antireflectivity by the formation of a microrelief with a greater contrast and optimised profile.

Acknowledgements. This work was partially supported by the competitiveness enhancement programme of the National Research Nuclear University 'MEPhI'.

References

1. Hobbs D.S., MacLeod B.D. *Proc. SPIE Int. Soc. Opt. Eng*., **5786**, 349 (2005).
2. McDaniel S., Hobbs D., MacLeod B., Sabatino E., Berry P., Schepler K., Mitchell W., Cook G. *Opt. Mater. Express*, **4**, 2225 (2014).
3. Hobbs D.S., MacLeod B.D., Sabatino E., Mirov S.B., Martyshkin D.V. *Proc. SPIE Int. Soc. Opt. Eng*., **8530**, 8530OP (2012).
4. Guo Z., Qu S., Ran L., Liu S. *Appl. Surf. Sci*., **253**, 8581 (2007).
5. Venkatakrishnan K., Sivakumar N.R., Tan B. *Appl. Phys. A*, **76**, 143 (2003).
6. Hee C.W., Ngoi B.K.A., Lim L.E.N., Venkatakrishnan K., Liang W.L. *Opt. Laser Technol*., **37**, 93 (2005).
7. Semaltianos N.G., Perrie W., French P., Sharp M., Dearden G., Logothetidis S., Watkins K.G. *Appl. Phys. A*, **94**, 999 (2009).
8. Hossein G.M., Meng-Jyun L., Ji-Bin H., Jeng-Ywan J. *Opt. Lasers Eng*., **81**, 97 (2016).
9. Ruf A., Berger P., Dausinger F., Hügel H. *J. Phys. D: Appl. Phys*., **34**, 2918 (2001).
10. Lapshin K.E., Obidin A.Z., Vartapetov S.K. *Proc. SPIE Int. Soc. Opt. Eng*., **6606**, 66060V (2007).
11. Ruf A., Breitling D., Berger P., Dausinger F., Hugel H. *Proc. SPIE Int. Soc. Opt. Eng*., **4830**, 73 (2003).
12. Yahng J.S., Nam J.R., Jeoung S.C. *Opt. Lasers Eng*., **47**, 815 (2009).
13. Wang X., Jia T., Li X., Li C., Feng D., Sun H., Xu S., Xu Z. *Chin. Opt. Lett*., **3**, 615 (2005).
14. Guay F., Ozcan L.C., Kashyap R. *Opt. Commun*., **281**, 935 (2008).
15. Kozlovsky V.I., Korostelin Yu.V., Landman A.I., Podmar'kov Yu.P., Frolov M.P. *Kvantovaya Elektron*., **33**, 408 (2003) [*Quantum Electron*., **33**, 408 (2003)].
16. Frolov M.P., Korostelin Yu.V., Kozlovsky V.I., Mislavskii V.V., Podmar'kov Yu.P., Savinova S.A., Skasyrsky Ya.K. *Laser Phys. Lett.*, **10**, 125001 (2013).

17. Kozlovsky V.I., Korostelin Yu.V., Landman A.I., Mislavskii V.V., Podmar'kov Yu.P., Skasyrsky Ya.K., Frolov M.P. *Kvantovaya Elektron*., **41**, 1 (2011) [*Quantum Electron*., **41**, 1 (2011)].
18. Akimov V.A., Kozlovsky V.I., Korostelin Yu.V., Landman A.I., Podmar'kov Yu.P., Skasyrsky Ya.K., Frolov M.P. *Kvantovaya Elektron*., **38**, 205 (2008) [*Quantum Electron*., **38**, 205 (2008)].
19. Akimov V.A., Frolov M.P., Korostelin Y.V., Kozlovsky V.I., Landman A.I., Podmar'kov Y.P., Skasyrsky Y.K., Voronov A.A. *Appl. Phys. B*, **97**, 793 (2009).
20. Akimov V.A., Kozlovsky V.I., Korostelin Yu.V., Landman A.I., Podmar'kov Yu.P., Frolov M.P. *Kvantovaya Elektron*., **34**, 185 (2004) [*Quantum Electron*., **34**, 185 (2004)].
21. Gubin M.A., Kireev A.N., Kozlovsky V.I., Korostelin Yu.V., Lazarev V.A., Pnev A.B., Podmar'kov Yu.P., Tyurikov D.A., Frolov M.P., Shelkovnikov A.S. *Kvantovaya Elektron*., **42**, 565 (2012) [*Quantum Electron*., **42**, 565 (2012)].
22. Atezhev V.V., Vartapetov S.K., Zhukov A.N., Kurzanov M.A., Obidin A.Z. *Kvantovaya Elektron*., **33**, 689 (2003) [*Quantum Electron*., **33**, 689 (2003)].